Synthesis of minerals

Kovalsky G.A.[1], Kovalskaya T.N.[1], Ermolaeva V.N.[1,2], Chukanov N.V.[3], Ermolaev D.N.[1], Varlamov D.A.[1], Chaychuk K.D.[1], Behelev D.B.[1], Pekov I.V.[4]

Influence of mineral-forming composition on stability of zirconosilicates under different alkalinity conditions (according to experimental data).

[1]IEM RAS, Chernogolovka, [2]GEOKHI RAS, Moscow, [3]FRC PCP MC RAS, Chernogolovka, [4]Lomonosov MSU, Moscow tatiana76@iem.ac.ru

Abstract. A series of experiments on the synthesis of zirconosilicates were carried out at temperatures of 550–600°C and a pressure of 2 kbar for 10–14 days under conditions of varying alkalinity of the mineral-forming fluid (in solutions of 1 M NaCl + 6% NaOH, 1 M NaCl + 11.5% NaOH, 1 M NaCl + 23% NaOH, 46% NaOH, 1 M NaF + 5% NaOH, 10%, 20%, and 30% NaOH). The synthesis was carried out from stoichiometric mixtures corresponding, in bulk chemical composition, to eudialyte, låvenite, and zirsinalite. In a number of experiments, natural raslakite, a calcium-deficient eudialyte-group mineral (EGM), was used as a seed in an amount of 0.5–1.5 wt.% of the total charge. Based on the results of studies of the composition and structure of the experimental products (data of electron probe microanalysis, powder X-ray diffraction, and IR spectroscopy), conclusions were drawn about the crystallization conditions of zirconosilicates of various structural types.A comparative analysis of the experimental results with geological and mineralogical observations on zirconium mineralization in highly alkaline rocks was conducted.

***Keywords**: mineral synthesis, zirconosilicates, eudialyte group minerals, lovozerite group minerals, lovenite-type phases, vlasovite, parakeldyshite*

Alkaline, primarily sodium (± Ca) zirconosilicates (minerals of the eudialyte and lovozerite groups, låvenite, vlasovite, parakeldyshite) are characteristic components of agpaitic rocks, where they act as the main concentrators of zirconium. The content of eudialyte-group minerals in alkaline massifs sometimes reaches tens of percent of the total rock volume. The literature notes that a striking visual feature of the ultra-agpaitic stage (Kalk > 40%) is the presence of replacement rims of zirsinalite and other lovozerite-group minerals (LGM) around eudialyte grains (Khomyakov, 1990; Khomyakov, 1995). However, experimental studies have shown that the most highly alkaline eudialyte-group minerals (EGM) can crystallize together with LGM (Kovalskaya et al., 2023; Kovalskaya et al., 2024). Preliminary experiments on the hydrothermal synthesis of eudialyte and a number of other zirconosilicates have shown (Kovalskaya et al., 2023; Kovalskaya et al., 2023; Kovalskaya et al., 2025) that the phase composition of the reaction products and the chemical composition of the phases therein depend critically primarily on the overall chemical composition of the reaction mixture, even minor changes of which can lead to very significant changes in the phase and chemical composition of the products.

This paper characterizes the results of experiments on the synthesis of zirconosilicates in reaction systems of multi-element composition. The starting materials used were sol-gels of eudialyte, zirsinalite, and låvenite stoichiometry, prepared using the gel method. The initial solutions used were 1M NaCl, 1M NaF, 1M NaCl + 46% NaOH, 1M NaCl + 23% NaOH, 46% NaOH, 1M NaCl + 6% NaOH, 1M NaCl + 11.5% NaOH, 10, 20, and 30% NaOH, 1M NaF + 10% Na_2CO_3, and 1M NaF + 5% NaOH. In some experiments, a natural EGM – raslakite – was used as a seed in an amount of 0.5–1.5 wt.% of the charge mass. The experiments were conducted in platinum ampoules using a high-pressure gas apparatus (designed at IEM RAS) at temperatures of 550–600°C and a pressure of 2 kbar. The charge, the seed (where necessary), and the solution were loaded into ampoules, which were then sealed and checked for leaks. The duration of the experiments was 10–14 days. The chemical composition of the solid reaction products was studied by electron probe microanalysis. Typical chemical compositions of the zirconosilicates obtained during the experiments are presented in Table 1.

According to electron probe microanalysis, powder X‑ray diffraction, and IR spectroscopy data, the synthesis using a mixture of 1M NaCl and 11.5% NaOH yielded eudialyte and vlasovite (Fig. 1). When using a mixture of 1M NaF with 10% Na_2CO_3, låvenite, its Ca,Fe-analogue, johansenite, Mn-bearing hematite, and calcite were formed (Figs. 2, 3). Upon adding a mixture of 1M NaF solution with 5% NaOH solution, låvenite, namansilite, aegirine, and Mn-bearing hematite were formed (Fig. 4). Using a 10% NaOH solution yielded vlasovite, zirsinalite, and pectolite (Fig. 5); using a 20% NaOH solution yielded vlasovite and a silicate of composition $Na_{1.42–1.44}Ca_{0.77–0.84}Zr_{0.38–0.47}Si_{3.00}O_x$ (Fig. 6); and using a 30% NaOH solution yielded vlasovite, parakeldyshite, pectolite, and a silicate of composition $Na_{1.32–1.55}Ca_{0.81–0.89}Zr_{0.38–0.44}Si_{3.00}O_x$ (Fig. 7). Thus, the experimental results show that under less alkaline conditions (using 5% NaOH solution or 10% Na_2CO_3 solution), låvenite-type phases (LTP) are formed, whereas under more alkaline conditions, eudialyte, zirsinalite, and vlasovite are formed.

The results of the experiments and their comparison with natural post-magmatic parageneses in alkaline massifs indicate the influence of the fluid regime on the composition of the crystallizing phases

under identical temperature and pressure conditions. When using initial solutions with 1M NaF and 5% NaOH (or 10% Na_2CO_3), låvenite and its Ca,Fe-analogue appear, whereas in a more alkaline solution (1M NaCl and 11.5% NaOH), eudialyte and vlasovite are formed. Using a 10% NaOH solution yields vlasovite, zirsinalite, and pectolite; using a 20% NaOH solution yields vlasovite and a silicate of composition $Na_{1.42-1.44}Ca_{0.77-0.84}Zr_{0.38-0.47}Si_{3.00}O_x$; and using a 30% NaOH solution yields vlasovite, parakeldyshite, pectolite, and a silicate of composition $Na_{1.32-1.55}Ca_{0.81-0.89}Zr_{0.38-0.44}Si_{3.00}O_x$. That is, with increasing alkalinity of the solution, zirsinalite does not form, but crystallization of parakeldyshite is observed, which under these experimental conditions served as an indicator of increased alkalinity of the mineral-forming environment.

Table 1. Chemical composition of some zirconosilicates obtained during the experiments.

Component	EGM	Zirsinalite	Parakeldyshite	LGM	elpidite	Vlasovite	LTP
			Content, wt.%				
Na_2O	19.11	24.20	17.28	8.40	8.41	13.51	10.69
K_2O	b.d.l.	b.d.l.	b.d.l.	1.29	b.d.l.	b.d.l.	b.d.l.
CaO	13.09	7.76	0.56	3.29	2.14	b.d.l.	10.56
MnO	b.d.l.	b.d.l.	b.d.l.	b.d.l.	b.d.l.	b.d.l.	10.99
FeO	0.94	1.04	1.18	2.79	b.d.l.	0.39	3.42
ZrO_2	10.61	15.03	41.91	18.68	22.70	28.86	31.84
TiO_2	b.d.l.	b.d.l.	b.d.l.	b.d.l.	b.d.l.	0.16	b.d.l.
SiO_2	54.27	51.71	39.68	58.21	58.66	56.34	29.22
Nb_2O_5	0.99	b.d.l.	b.d.l.	1.49	b.d.l.	1.45	b.d.l.
F	b.d.l.	b.d.l.	b.d.l.	b.d.l.	0.16	b.d.l.	2.44
$–O=F_2$	0	0	0	0	0.07	0	1.03
Cl	b.d.l.	b.d.l.	b.d.l.	b.d.l.	b.d.l.	b.d.l.	0.12
$–O=Cl_2$	0	0	0	0	0	0	0.03
Sum	99.03	99.74	100.61	94.15	92.01	100.71	98.22
			Formula coefficients				
Na	17.60	5.44	1.69	1.68	1.67	1.85	1.42
K	0	0	0	0.17	0	0	0
Ca	6.67	0.96	0.03	0.36	0.24	0	0.77
Mn	0	0	0	0	0	0	0.64
Fe	0.37	0.10	0.05	0.22	0	0.02	0.20
Zr	2.46	0.85	1.03	0.94	1.13	1.00	1.06
Ti	0	0	0	0	0	0.01	0
Si	25.78	6	2	6	6.00	4	2.00
Nb	0.22	0	0	0.07	0	0.05	0
F	0	0	0	0	0.06	0	0.53
Cl	0	0	0	0	0	0	0.02
Calcul. basis	Si + Nb = 26	Si = 6	Si = 2	Si = 6	Si = 6	Si = 4	Si = 2

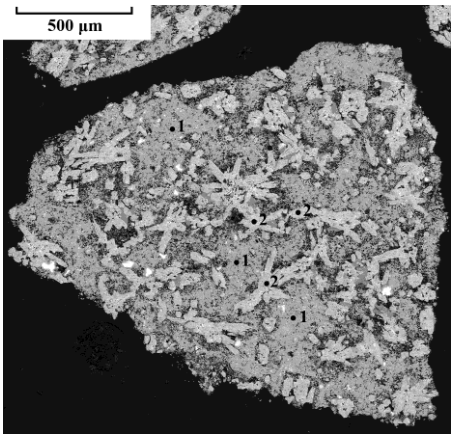

Figure 1. Products of experiment 62. 1 – eudialyte, 2 – vlasovite. Backscattered electron image of a polished section under a scanning electron microscope

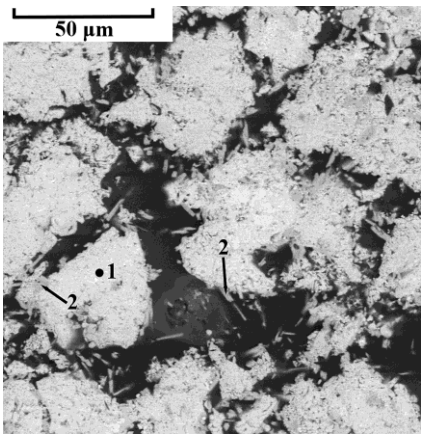

Figure 2. Products of experiment 96. 1 – låvenite, 2 – phase $CaMnSi_2O_6$. Backscattered electron image of a polished section under a scanning electron microscope.

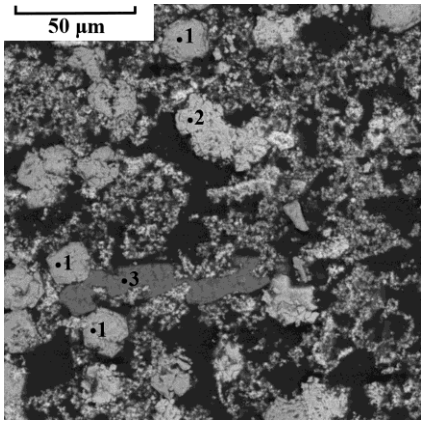

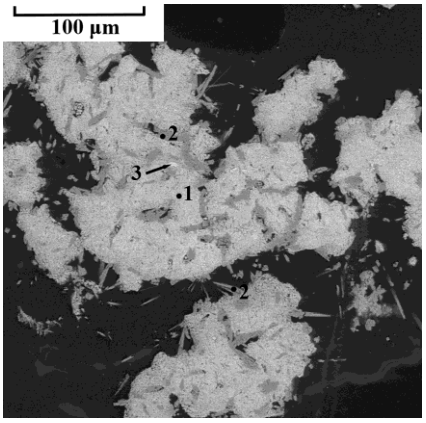

Figure 3. Products of experiment 98. 1 – Ca,Fe-analogue of låvenite, 2 – Mn-bearing hematite, 3 – calcite. Backscattered electron image of a polished section under a scanning electron microscope.

Figure 4. Products of experiment 97. 1 – låvenite, 2 – namansilite, 3 – Mn-bearing hematite. Backscattered electron image of a polished section under a scanning electron microscope.

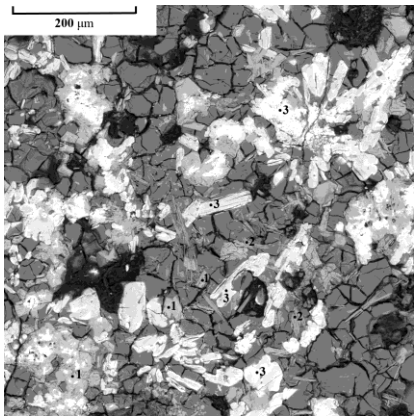

Figure 5. Products of experiment 87. 1 – zirsinalite, 2 – pectolite, 3 – vlasovite. Backscattered electron image of a polished section under a scanning electron microscope.

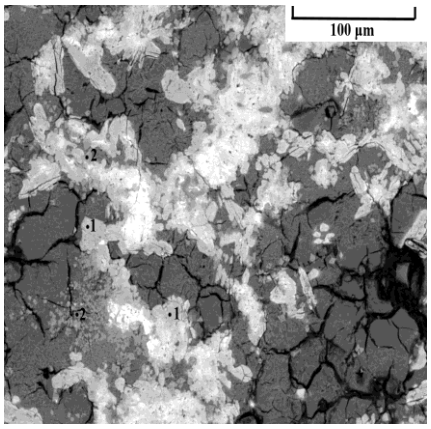

Figure 6. Products of experiment 88. 1 – vlasovite, 2 – pectolite. Backscattered electron image of a polished section under a scanning electron microscope.

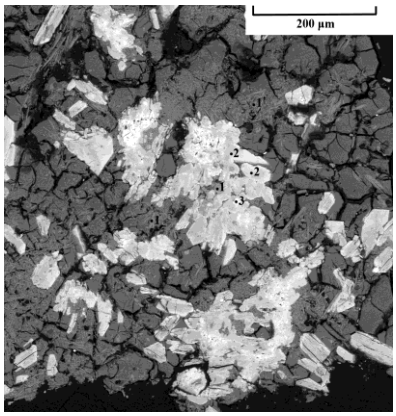

Figure 7. Products of experiment 89. 1 – pectolite, 2 – vlasovite, 3 – parakeldyshite. Backscattered electron image of a polished section under a scanning electron microscope.

It is interesting to note that in calcium-free experiments, eudialyte-group minerals (EGM) do not form, although almost calcium-free EGM occur in nature in ultra-agpaitic pegmatites; however, at low chlorine contents in the system, low-calcium EGM are formed. In the experimental products, eudialyte is associated either with elpidite and/or vlasovite, or with highly alkaline zirconosilicates (zirsinalite and/or parakeldyshite), and these associations do not overlap. EGM do not form from a charge of låvenite composition, which is also in good agreement with data on natural associations, where låvenite is also rarely found in close association with EGM. Parakeldyshite forms over a wide range of reaction mixture compositions, but only under high alkalinity conditions. Apparently, parakeldyshite has a very wide stability field, which definitely overlaps with the stability fields of EGM and lovozerite-group minerals (LGM).

The work was carried out within the framework of the state assignment of IEM RAS FMUF-2022-0002 and using budget funding from the V.I. Vernadsky Institute of Geochemistry and Analytical Chemistry of the Russian Academy of Sciences (GEOKHI RAS). The IR spectroscopic study, as well as (partially) the interpretation of analytical data, were performed in accordance with the state assignment (state registration number 124013100858-3), and the mineralogical studies were carried out within the framework of the state assignment of Lomonosov Moscow State University (topic No. 121061600049-4).

References

Kovalskaya T.N., Ermolaeva V.N., Chukanov N.V., Kovalskiy G.A., Varlamov D.A., Chaichuk K.D. Synthesis of zirconosilicates under high alkalinity conditions // Zapiski Rossiyskogo Mineralogicheskogo Obshchestva (Proceedings of the Russian Mineralogical Society). 2023. Vol. 152. No. 4. P. 123–134. DOI: 10.31857/S0869605523040068.

Kovalskaya T.N., Ermolaeva V.N., Chukanov N.V., Varlamov D.A., Kovalskiy G.A., Chaichuk K.D., Ermolaev D.N. Zircono- and titanosilicates as indicators of alkalinity in alkaline pegmatites (based on experimental data) // All-Russian Annual Seminar on Experimental Mineralogy, Petrology, and

Geochemistry (ARASEMPG-2025). Moscow, April 15–16, 2025. P. 49.
Khomyakov A.P. Mineralogy of Hyperagpaitic Alkaline Rocks. Moscow: Nauka. 1990. 196 p.
Kovalskaya T.N., Ermolaeva V.N., Chukanov N.V., Varlamov D.A., Kovalskiy G.A., Zakharchenko E.S., Kalinin G.M., Chaichuk K.D. Synthesis of Fe-deficient eudialyte analogues: Relationships between the composition of the reaction system and crystal-chemical features of the products. Mineralogical Magazine. 2023. Vol. 87. First View. P. 233–240. https://doi.org/10.1180/mgm.2023.1. DOI: 10.1180/mgm.2023.1.
Kovalskaya T.N., Ermolaeva V.N., Kovalskiy G.A., Varlamov D.A., Chukanov N.V., Chaichuk K.D. Synthesis of zirconosilicates under high alkalinity conditions. Experiment in Geosciences. 2024. Vol. 30. N 1. P. 83–86.
Khomyakov A.P. Mineralogy of Hyperagpaitic Alkaline Rocks. Oxford: Clarendon Press, 1995. 223 pp.

Redkin A.F.[1], Nekrasov A.N.[1], Neretina A.N.[1], Drozhzhina N.A.[1] Composition, properties and evolution of sodium and niobium oxy-fluorides at high temperature and pressure. *UDC 550.4.02+550.84+552.11*

[1] D.S. Korzhinsky Institute of Experimental Mineralogy of the Russian Academy of Sciences
redkin@iem.ac.ru;nekrasov@chgnet.ru; neretina-anna@yandex.ru;nadron@mail.ru

Abstract. Experimental studies of the interaction of Nb_2O_5 with 1 *m* NaF solutions at T = 680 – 800°C, p = 1 – 2 kbar, showed that during the chemical reaction sodium and niobium oxy-fluorides are formed, and the solution itself is significantly acidified. The products of the experiments are represented by crystals ranging in size from 2 to 100 microns, which, according to XRD and RS studies, correspond to pyrochlore-like and perovskite-like phases. The influence of temperature, pressure and interaction kinetics on the shape and structure of crystals is considered.

***Keywords**: experiment, pyrochlores, perovskites, XRD analysis, electron microscopy, Raman spectroscopy*

The formation of sodium and niobium oxy-fluorides was observed after interaction of Nb_2O_5 precursors and NaF solution under T = 680 – 800°C, p = 1 – 2 kbar. The Na/Nb ratio in the precursor was ~2.7. At 680°C, 1 kbar, the products of experiments were represented by crystals having an octahedron shape (fig. 1), and no other crystalline forms were found. Powder XRD of products in these experiments (fig. 2) corresponds to the pyrochlore-like phase (defect pyrochlore = Pcl-L) with structure *Fd3m* and LC (lattice constants) a=10.513 Å. According to the analysis on a scanning electron microscope, the newly formed Pcl-L phase had an average composition of $Na_{1.93}Nb_2O_{5.10}F_{1.73}$.

The products of experiments at 700 и 720°C, 1 kbar (fig. 2) were represented by both Pcl-L phases (C) with composition of $Na_{1.91}Nb_2O_{5.18}F_{1.54}$ and defect perovskites (O) $Na_{0.92}NbO_{2.93}F_{0.06}$. Moreover, with increasing temperature of experiments from 700 to 720 and further to 800°C, the amount of Pcl-L phase remarkably decreases (fig. 2, 3).

In experiments conducted at 800°C and pressure 2 kbar, only a sole phase Prv-L was detected in the products of experiments. Powder XRD of this phase corresponds to the orthorhombic crystal system. The spectrum analysis was performed using the FullProfSuit program [Rodríguez-Carvajal, 2001].

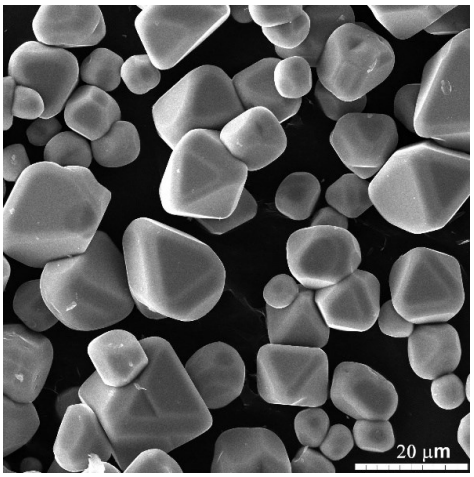

Fig. 1. SEM images of products of experiments at 680°C, 1 kbar.

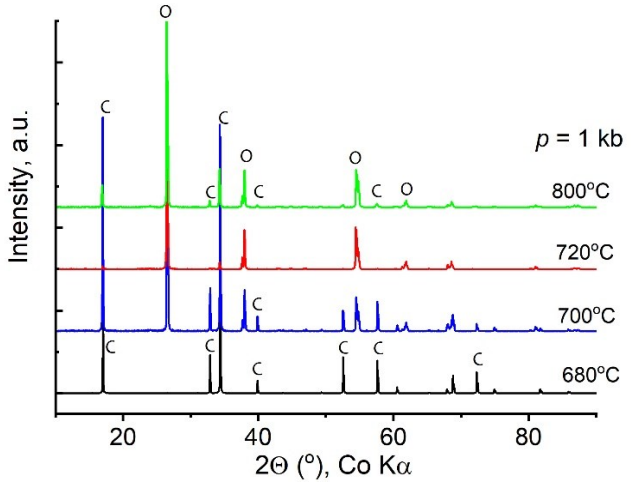

Fig. 2. XRD of products of interaction between Nb_2O_5 and 1.0 *m* NaF solutions. Abbreviations: c-cubic; o-orthorhombic.

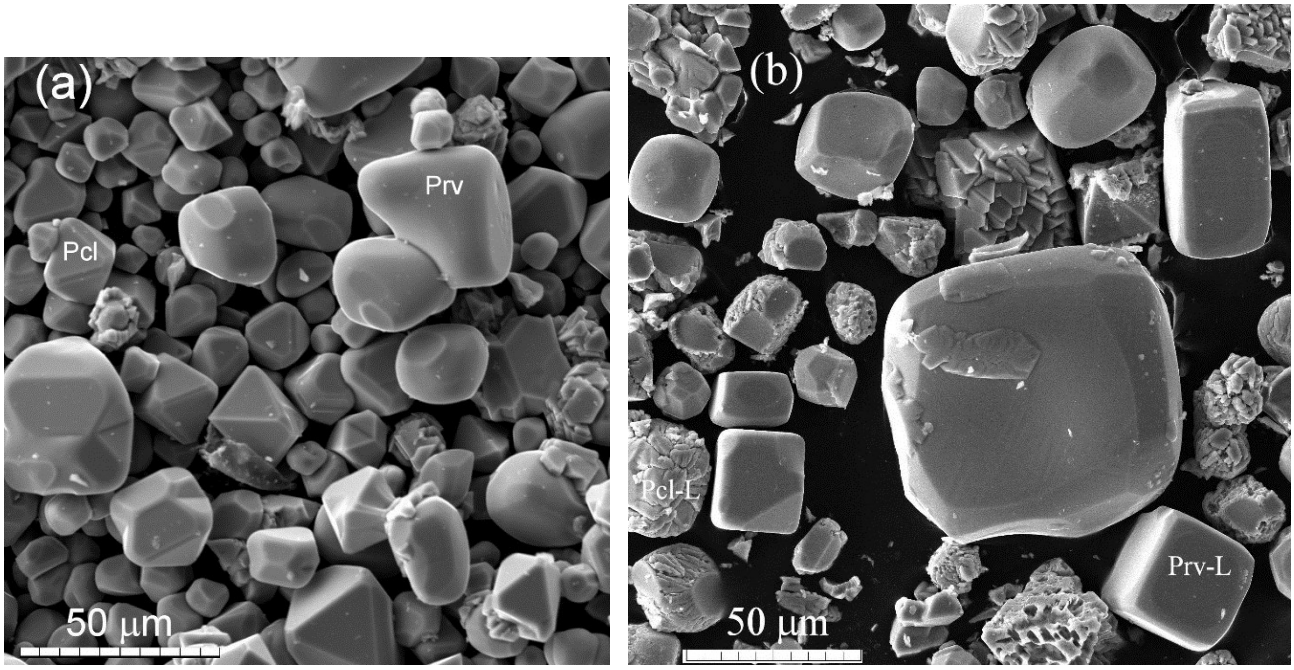

Fig. 3. SEM images of run products at 700°C (a) and 800°C (b), 1 kbar.

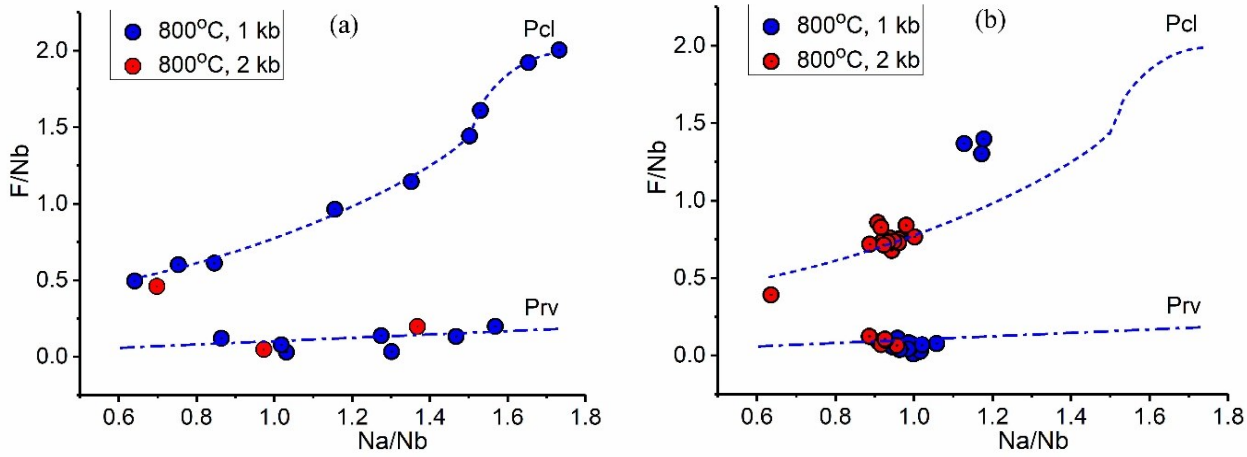

Fig. 4. Compositions of Pcl and Prv phases on the surface of crystals glued to CT (a) and on polished crystals in PS (b).

Fig. 4 shows the composition of Pcl and Prv phases on the surface of crystals glued to carbon adhesive tape (CT) and the slot is in polystyrene (PS) in the experiments, carried out at HPE at 800°C with Co–CoO buffers. The composition of Prv in the polished samples were found to be corresponded to the formula $Na_{1-x}NbO_{3-y}F_{2y}$. The fluorine content in perovskite is insignificant and is within a 3-fold error of the analysis, however, the presence of fluorine affects the habitus of crystals. The process of Prv crystal growth occurs due to the dissolution of Pcl crystals with removal of Nb^{5+} by acidic fluoride solutions. It leads to destruction of Pcl and formation of metastable phases containing an excess of Na and F over Nb.

The newly formed crystalline phases of Pcl and Prv at 680 – 800°C were studied by Raman spectroscopy at room temperature on a Renishaw spectrometer (RM1000) at a laser wavelength of 532 nm with a power of 2 MW in the wavenumber range from 100 to 4300 cm^{-1} with a step of 1.2 cm^{-1}. Raman spectra of the Pcl-L and Prv-L phases were significantly different (figs. 5–6), especially in the range of wave numbers in 130–500 cm^{-1}. The spectrum of Pcl-L is in good agreement with natural pyrochlore [Popova et al., 2022], whereas for the Prv-L phase, the wave numbers correspond to $NaNbO_3$ from the study [Ji et al., 2013].

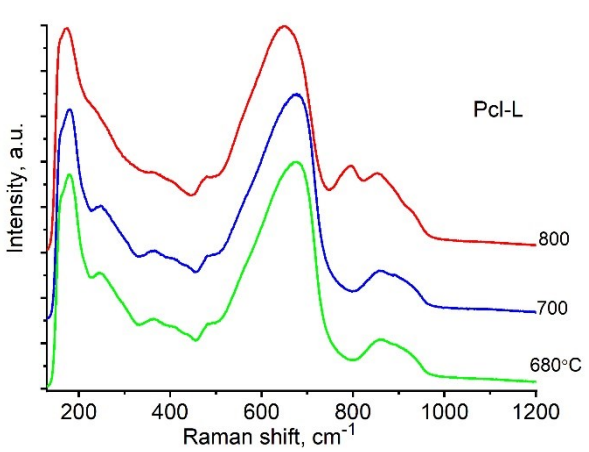

Fig. 5. The Raman spectra of the Pcl-L phases.

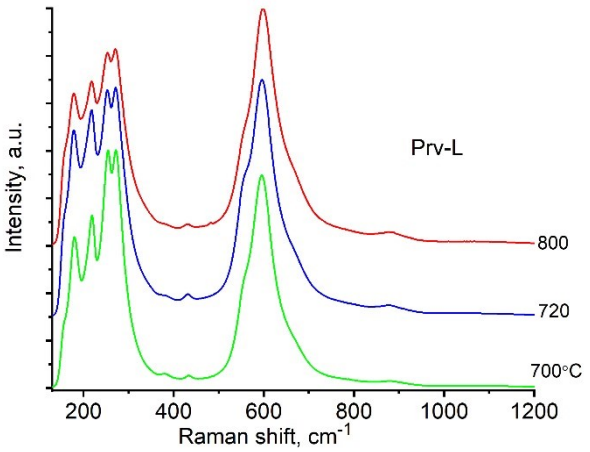

Fig. 6. The Raman spectra of the Prv-L phases**.**

According to the obtained data, perovskite is formed at 700°C. The rate of formation of both perovskite and pyrochlore from Nb_2O_5 in the solution of 1*m* NaF is significant, as evidenced by the absence of Nb_2O_5 in the products of experiments lasting 7 days. It is obvious that during the 2–3 hours required to heat the reactor to 690±10°C, a significant portion of the niobium pentoxide turns into pyrochlore, and the solution itself is acidified [unlike Boivin et al., 2022] due to the reaction

$Nb_2O_5 + (1.5+x)\ NaF + pH_2O + nH_2 \rightarrow Na_{1.5+x}Nb_2(O_{5+x}F_{1-y})F_{0.1+x+y}\cdot pH_2O + 0.4HF,$
where $n = 0.0$ at $y = 0$ and $n = 0.2$ at $y = 0.2$.

Upon further heating to 700–800°C and holding the experiments for 7 days, the unstable Pcl phase dissolves and the stable Prv phase grows.

In the experiment conducted in Internally Heated Pressure Vessel (IHPV) at 800°C and pressure 2 kbar, where it took only 15-20 minutes to bring the container with the ampoule to the specified *T-p* parameters, the amount of newly formed pyrochlore was insignificant and, after the experiment, it almost completely turned into perovskite.

The conducted studies have shown that the reaction Nb_2O_5 with 1 *m* NaF solutions leads to the formation of oxyfluorides Na-Nb and significant acidification of solutions. The composition and properties of the newly formed phases depend on *T*, *p* and fO_2. Pyrochlore-like octahedral crystals are formed at 680°C. At 700–800°C, crystals of a perovskite-like phase grow, estimated to be orthorhombic crystal system with a Bravais primitive lattice.

This work was supported by the Fundamental Research Program in the Russian Federation, projects FMUF-2022-0002 and FMUF–2022-0003

References

1. Boivin E., Pourpoint F., Saitzek S., SimonP., Roussel P., and Kabbour H. An unusual O^{2-}/F^- distribution in the new pyrochlore oxyfluorides: $Na_2B_2O_5F_2$ (*B* = Nb, Ta) // Chemical Communications, 2022, 58(14), 2391-2394. https://doi.org/10.1039/d1cc06760e
2. Ji S., Liu H., Sang Y., Liu W., Yu G., and Leng Y. Synthesis, structure, and piezoelectric properties of ferroelectric and antiferroelectric $NaNbO_3$ nanostructures // CrystEngComm, 2014, 16, 7598-7604. https://doi.org/10.1039/C4CE01116C
3. Popova, V.I., Popov, V.A., Blinov, I.A., Kotlyarov, V.A., and Lebedeva, S.M. A sequence of formation of «uranpyrochlore» and fluorocalciopyrochlore in alkali pegmatites from the Vishnevye Mountains, South Urals // Mineralogy, 2022, 8(2), 15-22. https://doi.org/10.35597/2313-545X-2022-8-2-2
4. Rodríguez-Carvajal J. Recent Developments of the Program FULLPROF, in Commission on Powder Diffraction (IUCr) // Newsletter. 2001, 26, 12–19.

Setkova T.V.[1], Verchenko P.A.[1], Spivak A.V.[1], Nekrasov A.N.[1] Crystal growth of Al-tourmaline – alumo-oxi-rossmanite analogue.

UDC: 549.612

[1] D.S. Korzhinskii Institute of Experimental Mineralogy Russian Academy of Sciences setkova@iem.ac.ru

Abstract. In this study, tourmaline crystals with a composition related to the synthetic analogue of alumino-oxy-rossmannite ($\square Al_3Al_6(Si_5AlO_{18})(BO_3)_3(OH)_3O$) were grown on a natural seed using a temperature gradient hydrothermal method at 600/650°C and 150 MPa. The newly formed colorless tourmaline layer in the pinacoid

direction reaches a thickness of 700 μm. Tourmaline of this composition, lacking predominant secondary divalent or trivalent cations, serves as an ideal reference standard for studying the structural and spectroscopic characteristics of the tourmaline supergroup.

***Keywords**: tourmaline, alumino-oxy-rossmannite, hydrothermal synthesis, crystal growth, Raman spectroscopy*

Tourmaline is a widespread borosilicate mineral has the ability to incorporate a wide variety of elements as mono-, di-, tri-, and tetravalent cations (Dutrow and Henry 2011). General formula is $XY_3Z_6T_6O_{18}(BO_3)_3V_3W$ where X = Na^+, K^+, Ca^{2+}, vacancy; $Y = Al^{3+}$, Cr^{3+}, V^{3+}, $Fe^{2+/3+}$, Mg^{2+}, Mn^{2+}, Li^+, Ti^{4+}; $Z = Al^{3+}$, Cr^{3+}, V^{3+}, $Fe^{2+/3+}$, Mg^{2+}; $T = Si^{4+}$, Al^{3+}, B^{3+}; $V = (OH)^-$, O^{2-}; $W = (OH)^-$, F^-, O^{2-}(Henry et al. 2011). Natural tourmaline samples are typically zoned, small, and chemically complex, which complicates the study of their structural and spectroscopic characteristics, including the incorporation of elements into specific structural positions. Studying synthetic tourmalines with simplified compositions facilitates the determination of these characteristics. Alumino-oxy-rossmannite (chemical formula $\square Al_3Al_6(Si_5AlO_{18})(BO_3)_3(OH)_3O$) (Ertl, et al. 2022) is a tourmaline group mineral with the minimum number of elements possible for tourmaline structure. In present work, crystal growth of Al-rich tourmaline with a composition close to alumino-oxy-rossmanite was carried out.

The experiments were performed in gold ampoules with a volume of 2 ml at a temperature of 600/650°C and a pressure of 100 MPa according to a previously developed method (Setkova et al. 2019, 2025). The nutrient mixture was prepared from Al_2O_3/SiO_2 oxides in a ratio of 1/1. The total weight of the solid oxide mixture was 1.5 g. In each experiment, a natural seed crystal was placed in the upper part of the ampoule to grow large tourmaline crystals suitable for comprehensive study. Solution was prepared based on boric acid and deionized water. The amount of solution was set by the filling factor of the ampoule, which, according to *PVT* diagrams, corresponded to a pressure of 100 MPa. The ampoule was placed in high gas pressure unit with internal heating.

The elemental composition and morphology of the phases obtained in the experiments were studied using a Tescan Vega II XMU scanning electron microscope (SEM) (Tescan, Czech Republic) with secondary and backscattered electron detectors for imaging and an INCA Energy 450 energy-dispersive spectrometer with an INCA x-sight Si(Li) semiconductor detector and an INCAWave 700 wave-dispersive spectrometer (Oxford Instruments, UK) for electron probe microanalysis (EPMA). For analysis, a flat-polished section of the sample and quartz was pressed in epoxy resin and sputtered with a carbon film. The analysis was performed at an accelerating voltage of 20 kV and an absorbed electron current of 56 nA in the Energy+ mode. For elements (O, Na, Mn, Al, Si, Ca, F) were determined using an energy-dispersive spectrometer (EDS), and the B content was simultaneously determined using a wavelength dispersive spectrometer (WDS). The EDS acquisition time was 70-100 seconds. The WDS data acquisition time was 40-100 seconds. Boron reference samples was $YAl_3(BO_3)$. Calculations of the analysis results were performed using the Microanalysis Suite Issue 18d +SP3 (INCA Suite version 4.15) software package. Oxygen contents were calculated based on the stoichiometry of the corresponding oxides. Quartz (SiO_2) was used as a reference sample for oxygen. The values of atoms per formula unit (apfu) of tourmaline were calculated for 15 cations in T, Z and Y sites, the H_2O by stoichiometry, the amounts of OH^- and O^{2-} in V and W positions by charge balance (based on the formula electroneutrality). Additionally, the B_2O_3 content was calculated stoichiometrically and compared with measured values. Raman spectra of the samples were collected using RM1000 (Renishaw) spectrometer with solid-state single-mode laser (wavelength of 532 nm). The secondary phases obtained in the experiments were determined by X-ray analysis on a Bruker Advance 8 diffractometer.

As a result of the experiments, a colorless layer up to 700 μm in thickness on the seed was obtained (Fig. 1a). SEM examination of the overgrowth layer showed that it is a homogeneous crystalline material (Fig. 1b) with composition close to ideal formula of natural mineral alumino-oxy-rossmanite (Table 1). The element distribution profile in the seed and overgrown layer was studied (Fig. 1). The seed corresponds to fluor-elbaite in composition (ideal formula $Na(Li_{1.5}Al_{1.5})Al_6(Si_6O_{18})(BO_3)_3(OH)_3F$) and is characterized by the presence of manganese and titanium cations. Synthetic tourmaline belongs to the vacant group, as there are no cations in the X-site. Aluminum occupies YO_3 and ZO_6 octahedra. A slight deficiency of silicon is observed in the T-site. Additionally, the TO_6 tetrahedra may contain aluminum or boron cations. The WDS data show that the boron content in the seed and overgrowth layer is coincides (Fig. 1c) and close in value with the calculated value for 3 apfu (Table 1). On the other hand, the silicon content correlates with aluminum. Therefore, it can be revealed that aluminum incorporated into TO_6 tetrahedra.

Table 1. Chemical composition (wt%) and atomic proportion in the chemical formula (apfu) of natural seed and synthesized Al-rich tourmaline

Component (wt%)		
	seed	overgrowth layer
SiO_2	37.27	35.17
TiO2	0.13	<d.l.
Al_2O_3	40.84	49.03
MnO	0.36	<d.l.
Li_2O*	1.75	0.00
CaO	1.72	<d.l.
Na_2O	1.34	<d.l.
B_2O_3	10.79	10.85
B_2O_3 (calc)	11.01	10.78
F	0.98	<d.l.
H_2O (calc)	3.29	4.34
Total	98.47	99.39

(*Y*+*Z*+*T*)=15 atoms per formula unit (apfu)			
		seed	overgrowth layer
X	Na	0.42	0.00
	Ca	0.30	0.00
	Vacancy	0.28	1.00
Y+*Z*	Al	7.49	9.00
	Li	1.45	0.00
	Mn	0.05	0.00
	Ti	0.01	0.00
T	Si	5.89	5.68
	Al	0.11	0.32
B	B	3.00	3.00
V+*W*	O	0.47	1.68
	OH	3.03	2.32
	F	0.50	0.00

*Li_2O content in seed crystal was estimated according A. Pesquera (Pesquera A. et al. 2016). d.l. = detection limit

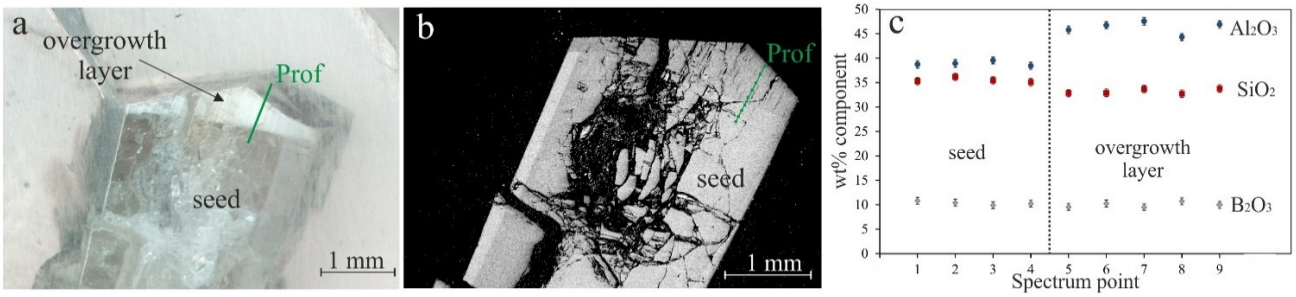

Fig. 1. (a) Growth of Al-rich tourmaline on natural seed; (b) SEM image of the seed and overgrowth layer, green line the profile of EPMA analysis; (c) element distribution (in wt% component) in seed and overgrowth layer according profile (a) and (b).

The Raman spectra of the natural seed and the overgrowth layer of Al-rich tourmaline were obtained in the range of 100-3800 cm^{-1} with bands of different intensities (Fig. 2). The bands have similar topology were distinguished to regions with corresponding vibrations (Watenphul et al, 2016). The main differences in regions of vibrations of the YO_6 and ZO_6 octahedron as well as ^{v}OH and ^{w}OH were observed.

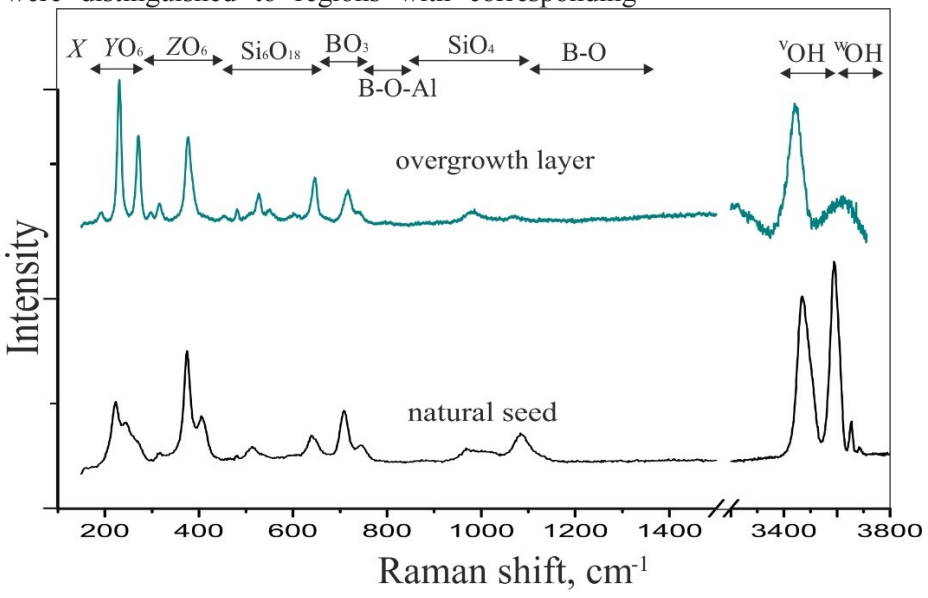

Fig.2. Raman spectra of overgrowth layer of Al-rich tourmaline in comparing with natural seed.

In results, tourmaline crystals with a composition close to alumino-oxy-rossmannite were successfully grown on natural seeds using a hydrothermal temperature-gradient method (600 / 650 °C, 150 MPa). The colorless overgrowth layer achieved a thickness of 700 μm in the pinacoid direction, providing an ideal, chemically simple reference standard for studying the structural and spectroscopic characteristics of the tourmaline supergroup.

The research was supported by RSF grant No. 25-27-00194 https://rscf.ru/project/25-27-00194/

References

Dutrow, B.L., and Henry, D.J. (2011) Tourmaline: A geologic DVD. Elements, 7, 301–306.

Ertl, A., John M. Hughes, J. M., Prowatke, S., Ludwig, T., Lengauer, C.L., Meyer, H., Giester, G., Kolitsch, U., Prayer, A. (2022) Alumino-oxy-rossmanite from pegmatites in Variscan metamorphic rocks from Eibenstein an der Thaya, Lower Austria, Austria: A new tourmaline that represents the most Al-rich end-member composition. American Mineralogist, 107, 157–166.

Henry, D.J., Novák, M., Hawthorne, F.C., Ertl, A., Dutrow, B.L., Uher, P., and Pezzotta, F. (2011) Nomenclature of the tourmaline-supergroup minerals. American Mineralogist, 96, 895–913.

Pesquera A., Gil-Crespo, P.P., Torres-Ruiz, F., Torres-Ruiz, J., Roda-Robles, E. (2016) A multiple regression method for estimating Li in tourmaline from electron microprobe analyses. Mineralogical Magazine, 80, 1129–1133.

Setkova, T. V., Balitsky, V.S., and Shapovalov, Y.B. (2019) Experimental study of the stability and synthesis of the tourmaline supergroup minerals. Geochemistry International, 57, 10, 1082–1094.

Setkova, T. V., Gorelova, L. A., Vereshchagin, O. S., Spivak, A. V., Verchenko, P. A., Vlasenko, N. S., Bocharov, V. N., Pankin D. V. (2025) Synthesis and crystal structure of V-rich tourmaline. American Mineralogist, 110, 12, 2042–2046.

Watenphul, A., Schlüter, J., Bosi, F., Skogby, H., Malcherek, T., Mihailova, B. (2016) Influence of the octahedral cationic-site occupancies on the framework vibrations of Li-free tourmalines, with implications for estimating temperature and oxygen fugacity in host rocks. American Mineralogist, 101, 11, 2554-2563.

Spivak A.V.[1], Setkova T.V.[1], Kuzyura A.V.[1], Zakharchenko E.S.[1], Bendeliani A.A.[2], Gornova E.S.[1,2], Bobrov A.V.[1,2], Vaitieva Y.A.[3], Aksenov S.M.[3], Synthesis and structural features of mica $K_2Mg_5(Si_4O_{10})_2(OH)_4$. *UDC 550.4.02*

[1]D.S. Korzhinskii Institute of Experimental Mineralogy of Russian Academy of Sciences, Chernogolovka, spivak@iem.ac.ru, setkova@iem.ac.ru, shushkanova@iem.ac.ru, egorzero@gmail.com,
[2] Geological Faculty, Lomonosov Moscow State University, Moscow wodanite@gmail.com, sk0rlupka@yandex.ru archi3@yandex.ru
[3] Laboratory of Arctic Mineralogy and Materials Sciences, FRC Kola Science Centre of Russian Academy of Sciences, Apatity yulia.vaitieva@yandex.ru, aks.crys@gmail.com

Abstract. Synthetic high-silica mica with the chemical formula $K_2Mg_{5.019}Al_{0.03}1Si_{7.949}O_{20}(OH)_4$ was obtained as spontaneous crystals up to 1 mm in size by hydrothermal synthesis at 600-650 °C and 150 MPa in a high gas pressure vessel (IEM RAS). By the chemical composition the synthesized mica corresponds to Mg-analogue of montdorite and (OH)-analogue of yangzhumingite. Unit cell parameters of synthetic mica: a = 5.2599 (1) Å, b = 9.1056 (1) Å, c = 10.1917 (1) Å, β = 99.969 (1)°, space group $C2/m$. The structure is characterized by a trioctahedral arrangement, with magnesium distributed across the octahedral $M1$ and $M2$ positions. The tetrahedral layers are predominantly occupied by silicon, with aluminum appearing only as a minor impurity, allowing the synthesized phase to be classified as a high-silica micas.

Keywords: *mica, tetrasilicic mica, synthesis, single crystal XRD*

Introduction. Micas are a large group of phyllosilicate minerals with a layered structure and the general formula $A_2M_{4-6}T_8O_{20}X_4$, where A is K, Na or Ca or less commonly Ba, Rb, or Cs; M is Al, Mg, or Fe or less commonly Mn, Cr, Ti, Li, etc.; T is chiefly Si or Al, but also may include Fe^{3+} or Ti; X is OH, F (Feininger, 2003; Rieder et al., 1999). Phyllosilicate with the composition $K_2Mg_5(Si_4O_{10})_2(OH)_4$ was first synthesized by Seifert F. and Schreyer W. in 1965 (Seifert and Schreyer, 1965). In addition, a F-analogue $KMg_{2.5}Si_4O_{10}F_2$ of this phase was synthesized from the melt at 1400°C by cooling to 1100 °C (Toraya et al., 1976). Later, minerals corresponding to these synthetic analogues were found in nature. One of them was named "montdorite" in honor of the Mont Dore stratovolcano (France), in whose rocks it was discovered (Robert and Maury, 1979). Another member of the mica group is yangzhumingite with the ideal formula is $KMg_{2.5}Si_4O_{10}F_2$. Through its tetrasilicic, fluorine-dominant and interlayer K-dominant character, yangzhumingite represents the Mg-analogue of montdorite.

The object of this study was synthetic tetrasilicic mica, a Mg-analogue of montdorite or (OH)-analogue of yangzhumingite. The objectives of the study are to synthesize crystals of synthetic tetrasilicic mica of the required quality for structural studies and refine the structure using the single crystal XRD.

Methods. The synthesis was carried out in the hydrothermal gradient conditions at temperature 600/650 °C and pressure of 150 MPa on high gas pressure vessels with internal heating. The

advantages of using this setup are that gas pressure vessels have a large internal volume and a wide controller zone as gradient and gradient-free. The temperature was determined with an accuracy no higher than ±5°C according to the calibration curve using $Pt_{30}Rh/Pt_6Rh$ thermocouples with an electrode thickness of 0.3 mm, the junction of which was inserted into the two position of gradient zone with higher 650°C and lower 600°C temperature. The pressure in the system was set by the Ar gas. An aurum ampule volume of 2 ml was used. The starting composition (0.5g) consisted of oxides MgO (99.96), Al_2O_3 (99.96) and SiO_2 (99.96) in a ratio close in stoichiometry to phlogopite ($KMg_3AlSi_3O_{10}(OH)_2$), at that magnesium and aluminum oxides were a powdered and silica in the form of a quartz crystal rod. The ampoule was filled with a 5 wt% KOH solution based on deionized water in an amount corresponding to the filling factor (Wagner and Pruss, 2002) that according to pressure 150 MPa. The ratio of the solution and solid phases was 1:2. The duration of the experiments was 14 days. Morphology of the obtained crystals was studied by optical (MBS-9, ADF STD16, and Nikon Eclipse LV100pol) and scanning electron (Tescan Vega II XMU) microscopy.

The chemical compositions of experimental samples were determined by electron probe microanalysis (EPMA) using Tescan - VegaIIXMU electron microscopy with INCA Energy 450 energy dispersive spectrometer (EDS), equipped with an INCA x-sight semiconductor Si (Li) detector and an INCA Wave 700 wavelength-dispersive spectrometer (WDS) (Oxford Instruments) at IEM RAS. Polished samples were preliminarily coated with ~15 μm carbon film. The microprobe measurements were carried out at an accelerating voltage of 20 kV, a focused beam current of ~10 nA, and counting times of 70s. The following standards were used: Si – SiO_2, Mg - MgO, Al – Al_2O_3, Fe - iron metal and K - orthoclase.

Crystals were selected under a polarizing light microscope and attached to glass fibers. The data were collected at ambient temperature on a Rigaku XtaLAB Synergy-S single-crystal diffractometer (ω-scan mode) with a graphite monochromatized Mo*K*α radiation source (λ = 0.71073 Å) and a Hybrid Pixel Array detector. Unit cell parameters were determined and refined, a semi-empirical absorption correction based on the intensities of equivalent reflections was applied, and the data were corrected for Lorentz, polarization, and background effects using CrysAlis software ("Rigaku Oxford Diffraction, CrysAlisPro Software system, version 1.171.41.97a," 2021). The refinements of the structures were carried out using the Jana2006 software package (Petricek et al., 2014).

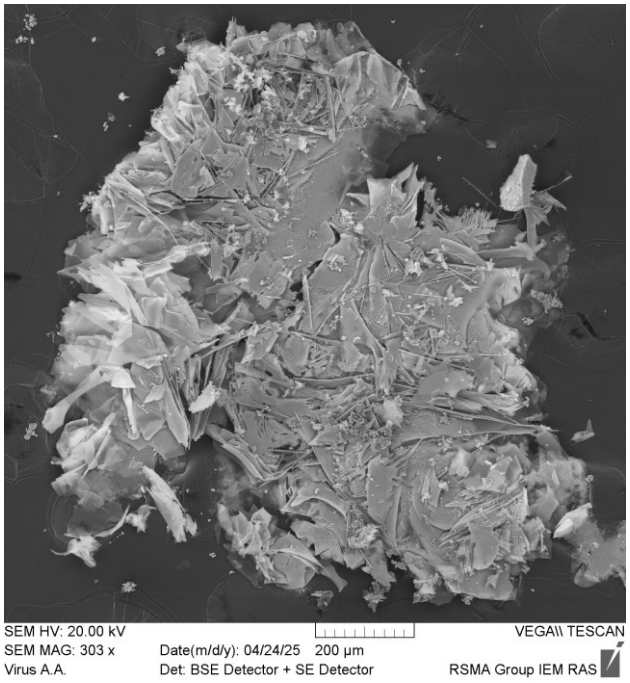

Fig. 1. SEM images of crystals of synthetic mica.

Results and discussion. Colorless, transparent mica crystals up to 1 mm in size were synthesized (fig. 1). The formation of these crystals was largely concentrated at the contact zone with the quartz rod, which provided the silica necessary for the mica. The morphology and chemical composition of the mica crystals do not depend on their location in the upper or lower growth zone. The obtained mica crystals are characterized by a homogeneous composition. By the variations in the Al and Si contents in mica, the compositions of the synthesized mica correspond to the composition of the end-member montdorite/yangzhumingite: 58.69 SiO_2, 0.37 Al_2O_3, 24.94 MgO, 11.16 wt%K_2O.

The crystal structure was refined in monoclinic symmetry (sp. gr. *C*2/*m*) with lattice parameters: a = 5.2599 (1)Å, b = 9.1056 (1) Å, c = 10.1917 (1) Å, β = 99.969 (1)°. The crystal-chemical formula obtained based on the structural data is (Z=2): $^{A}K[^{M1}(Mg_{0.818}\square_{0.182})\ ^{M2}(Mg_{0.846}\square_{0.154})_2\ ^{X}(OH_{0.986}\square_{0.014})_2][^{T1,2}(Si_{0.994}Al_{0.004}\square_{0.002})_2O_5]_2$, where □ is the vacancy and the square brackets show the composition of the *O*- and *T*-layers.

In micas with space group *C*2/*m*, the *M*1 site corresponds to the Wyckoff position *c*, with multiplicity of 2 and site symmetry of 2/*m* (Sokolova et al., 2018). The crystal structure of the synthetic mica $K_2Mg_5(Si_4O_{10})_2(OH)_4$ is similar to that of other 1*M* polytypes of trioctahedral micas and is based on the triple-layered *TOT*-modules (Fig. 2) (Backhaus and Durovic, 1984; Chukanov et al., 2019; Ferraris and Ivaldi, 2002; Nespolo and Durovic, 2002). These modules contain central *O*-layer of edge-sharing

*M*φ$_6$-octahedra (where φ denotes the anionic ligand, represented by O^{2-}, OH^-) and two tetrahedral *T*-layers.

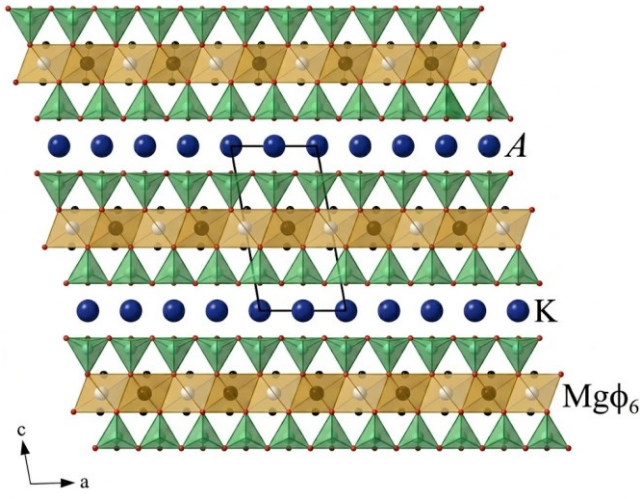

Fig 2. General view of the crystal structure of the synthetic mica with the general formula $K_2Mg_5(Si_4O_{10})_2(OH)_4$ projected onto the *ac* plane

In the structure of new synthetic mica *O*-layer is formed by two kinds of *M*φ$_6$-octahedra with similar chemical composition. The *M*1φ$_6$-octahedron (<*M* – φ > = 2.062 – 2.093 Å) is occupied by Mg (0.818 apfu) and features a vacancy (0.182 apfu). The *M*2φ$_6$-octahedron (<*M* – φ > = 2.068 – 2.089 Å) is occupied by Mg (0.846 apfu) and features a vacancy (0.154 apfu). The similar <*M* – φ > distances and vacancy fractions suggest a lack of long-range ordering between the two octahedral sites.

Tetrahedral *T*-layers are formed by *T*O$_4$-tetrahedra (<*T* – O> = 1.596 – 1.638 Å) which are occupied by silicon, while aluminum is a minor impurity phase. The triple-layer *TOT* modules are linked by the interlayer *A*-site (<*A* – φ>=3.094 Å) which is located in the center of a large 12-vertex polyhedron predominantly occupied by K. The *X*-site is occupied by OH^- linked to the oxygen atom of the *M*φ$_6$-octahedron by weak hydrogen bond (with *D*···*A* distances of about 3.05 Å).

Polytypism in micas is known to be controlled by their variable chemistry, as well as by specific filling of the O layer. Furthermore, pressure and temperature have a significant impact on the distortions of coordination polyhedra (Ferraris and Ivaldi, 2002; Zanazzi and Pavese, 2002). Thus, a wide variability of micas is both due to changes in the chemistry of the mineral-forming media and changes in intensive parameters. The combined information on the chemical composition and crystal chemistry of micas allows us to consider this mineral as an indicator of the geological regimes and peculiarities of mineral-forming systems.

Conclusions.

This study demonstrates the successful hydrothermal synthesis of large (up to 1 mm), high-quality transparent mica crystals using high gas pressure vessels at 600/650 °C and 150 MPa. The experimental conditions and the use of a quartz rod as a silica source facilitated the growth of homogeneous crystals with chemical composition corresponded to magnesian end-member of montdorite and (OH)-analogue of yangzhumingite.

Single-crystal X-ray diffraction analysis confirmed that the synthetic mica, with the refined formula $K_2Mg_{5.019}Al_{0.031}Si_{7.949}O_{20}(OH)_4$, crystallizes in the *C*2/*m* space group with unit cell parameters: *a* = 5.2599 (1)Å, *b* = 9.1056 (1) Å, *c* = 10.1917 (1) Å, *β* = 99.969 (1)°. The structure is characterized by a trioctahedral arrangement where magnesium vacancies are distributed across both the *M*1 and *M*2 octahedral sites. The lack of long-range ordering between these sites, supported by similar bond distances and vacancy fractions, suggests a stable yet flexible lattice. The tetrahedral layers are predominantly occupied by silicon, with aluminum acting only as a minor impurity, reinforcing the tetrasilicic nature of the synthesized phase.

Thus, the combination of advanced hydrothermal synthesis, structural refinement has allowed for the characterization of a pure synthetic mica. These findings contribute to the broader understanding of trioctahedral mica stability and crystal chemistry, providing a robust model for investigating the role of octahedral vacancies and tetrasilicic substitution in phyllosilicates.

Acknowledgments. This study is fulfilled under Research program № FMUF-2022-0001 and № FMUF-2022-0002of IEM RAS and № 122011300125-2 of KSC RAS, RSF grant № 24-77-00031.

References

Backhaus K.-O., Durovic S. Polytypism of micas. I. MDO polytyper and their derivation // Clays Clay Miner. – 1984. – Vol. 32. – P. 453–463. https://doi.org/10.1346/CCMN.1984.0320603

Chukanov N.V, Aksenov S.M., Kasatkin A.V, Škoda R., Nestola F., Nodari L., Ryanskaya A., Rastsvetaeva R. 3 T polytype of an iron ‑ rich oxyphlogopite from the Bartoy volcanic field , Transbaikalia : Mössbauer , infrared , Raman spectroscopy, and crystal structure // Phys. Chem. Miner. – 2019. – Vol.46. https://doi.org/10.1007/s00269-019-01049-7

Feininger T. Rock-Forming Minerals. 3A. Sheet Silicates: Micas. – 2nd edition. – The Geological Society. – London. – 2003. https://doi.org/doi.org/10.2113/gscanmin.43.2.837-a

Ferraris G., Ivaldi G., Structural Features of Micas // Rev. Mineral. Geochemistry. – 2002. – Vol. 46. – P. 117–153. https://doi.org/10.2138/rmg.2002.46.03

Nespolo M., Durovic S. Crystallographic basis of Polytypism and Twinning in Micas // Rev. Mineral. Geochemistry. – 2002. – Vol. 46. – P. 155–279. https://doi.org/10.2138/rmg.2002.46.04
Petricek V., Dusek M., Palatinus L., Crystallographic Computing System JANA2006 : General features // Zeitschrift für Krist. – 2014. – Vol. 229. – P. 345–352. https://doi.org/10.1515/zkri-2014-1737
Rieder M., Cavazzini G., D'yakonov Y.S., Gottardi G., Koval' P.V., Muller G., Neiva A.M.R., Radoslovich E.W., Robert J.L., Sassi F.P., Takeda H., Weiss Z., Wones D.R. Nomenclature of the micas // Mineral. Mag. – 1999. – Vol. 63. – P. 267–279. https://doi.org/10.1180/002646199548385
Rigaku Oxford Diffraction, CrysAlisPro Software system, version 1.171.41.97a, 2021.
Robert J.L., Maury R.C. Natural Occurrence of a (Fe, Mn, Mg) Tetrasilicie Potassium Mica // Contrib. to Mineral. Petrol. – 1979. – Vol. 68. – P. 117–123.
Seifert F., Schreyer W. SYNTHESIS OF A NEW MICA, $KMg_{2.5}[Si_4O_{10}]D(OH)_2$ // Am. Mineral. – 1965. – Vol. 50. – P. 1114–1118.
Sokolova E., Hawthorne F.C., Agakhanov A.A., Pautov L.A., Karpenko V.Y.. The crystal structure of orlovite, $KLi_2Ti(Si_4O_{10})(OF)$: the first example of the short-range order of Ti in true trioctahedral micas // Eur. J. Mineral. – 2018. – Vol. 30. – P. 399–402. https://doi.org/10.1127/ejm/2018/0030-2724
Toraya H., Iwai S., Marumo F., Daimon M., Kondo R. The crystal structure of tetrasilicic potassium fluor mica, $KMg_{2.5}Si_4O_{10}F_2$ // Zeitschrift fur Krist. – 1976. – Vol. 144. – P. 42–52.
Wagner W., Pruss A. Revised Release on the {IAPWS} Formulation 1995 for the Thermodynamic Properties of Ordinary Water Substance for General and Scientific Use // J. Phys. Chem. Ref. Data. – 2002. – Vol. 31. – P. 387–535.
Zanazzi P.F., Pavese A. Behavior of Micas at High-Pressure and High-Temperature // Rev. Mineral. Geochemistry. – 2002. – Vol. 46. – P. 99–116. https://doi.org/10.2138/rmg.2002.46.02